The polarization of charge in the M=C_{carb} bond is calculated to be Cr(+0.80)-C(-0.19) and Fe(+0.52)-C(-0.22) for the Cr and Fe carbenes, respectively (values in parentheses show the gross atomic charge), though the electron is relatively deficient in the π region of the carbene carbon atom. Spangler et al.[8] also reported the gross charge Ni(+0.53)-C(-0.58) for $(CO)_3Ni{=}CH_2$. The carbene carbon is calculated to be negatively charged, in contradiction with the common idea based on the NMR ^{13}C chemical shift, large dipole moment, and reactivity (nucleophilic attack on carbene carbon). Though we have not yet calculated the ^{13}C chemical shift from the present MO's, the other two facts are well explained by the present calculations. The dipole moments of the complexes are calculated to be large and the reactivity of the complexes is not charge controlled but frontier controlled. The LUMO's of the complexes have large coefficient at the pπ AO of the carbene carbon atom. Between the Cr and Fe complexes, the Fe complex seems to be more reactive than the Cr complex from both the magnitudes of the MO coefficient and the orbital energy of the LUMO.

Acknowledgment. For the SCF calculations, we have used a slightly modified version of the HONDOG program due originally to King, Dupuis, and Rys whom the authors acknowledge. Calculations were carried out with the M-200 computers at the Institute for Molecular Science and the Data Processing Center of Kyoto University. This work was supported in part by a Grant-in-Aid for Scientific Research from the Japanese Ministry of Education, Science, and Culture.

Registry No. $(CO)_5Cr{=}CH(OH)$, 83998-88-3; *eq*-$(CO)_4Fe{=}CH(OH)$, 83998-89-4; *ax*-$(CO)_4Fe{=}CH(OH)$, 84026-47-1.

Covalent Bonding in *trans*-Tetraamminedinitronickel(II) Studied by X-ray Diffraction at 110 K

B. N. Figgis,* P. A. Reynolds, and S. Wright

Contribution from the School of Chemistry, University of Western Australia, Nedlands, Australia 6009. *Received April 2, 1982*

Abstract: The electron distribution of *trans*-tetraamminedinitronickel(II), $Ni(NH_3)_4(NO_2)_2$, has been studied at 110 K by single-crystal X-ray diffractometry. The data were analyzed by conventional least-squares methods and also by use of a model in which chemically reasonable appropriate s, p, and d hybrids were refined on all atoms. This gave R = 1.7%, R_w = 3.1% with $((\sin\theta)/\lambda)_{max}$ = 8.5 nm^{-1}. The model shows a substantial (0.38 (8) electron) σ donation of electrons from each nitrite to nickel, with no significant π contribution. The ammonia molecules each donate 0.11 (6) σ electron, which is, as expected, less than that from the nitrite ions. The valence density around the nickel is mainly 3d-like as expected (3d = 7.6 (1)), but there is a substantial 4p component (4p = 1.61 (2)). This gives a net charge on nickel of +0.8 (1). The aspherical distribution of this 3d density around the nickel atom is $3d_{xy}^{1.28(7)}3d_{yz}^{1.80(6)}3d_{xz}^{1.31(6)}3d_{z^2}^{1.36(8)}3d_{x^2-y^2}^{1.84(7)}$. This is the result expected from ligand-field theory if one takes into account the effects of covalence, except for an anomalously low d_{xz} population. The 4p electron density around the nickel atom is of orthorhombic rather than the expected tetragonal symmetry. The residual electron density also shows a further small diffuse component around the nickel atom not of 4s or 4p symmetry and features in the nitrite N-O bonds probably associated with overlap density.

The determination of both the electron density by X-ray diffraction and of spin density by polarized neutron diffraction in a single simple transition-metal complex should provide a stringent test of current theories of the electronic structure of such molecules. This is because the theories largely have been constructed to account for energetic (spectroscopic) observations not spatial (diffraction) ones. Although the effects of covalence are small in both experiments, they can be determined sufficiently well to provide new information of chemical interest. Examples are (phthalocyaninato)manganese(II)[1] and tricesium tetrachlorocobaltate(II) chloride[2] for spin densities and chromium hexacarbonyl,[3] iron pyrites,[4] and hexaamminecobalt(III) hexacyanochromate(III)[5] for charge densities.

Crystals of compounds suitable for both experiments must have a simple crystal structure, a substantial magnetic moment at 4.2 K, contain no elements highly absorbing for either X-rays or thermal neutrons, and suffer little extinction or anharmonicity in thermal motion. Crystals of *trans*-tetraamminedinitronickel(II), $Ni(NH_3)_4(NO_2)_2$, not only satisfy these restrictions, but the molecule is chemically interesting in that the nitrite anion, being high in the spectrochemical series, is expected to exert a substantial covalent effect.

Preliminary X-ray diffraction,[6,7] magnetochemical,[7,8] spectroscopic,[7] and neutron diffraction[9] experiments on this compound reveal no untoward features, such as structural or magnetic phase changes, or excessive extinction, although twinning is common. The present publication is devoted to an analysis of the X-ray diffraction data. Subsequent publications will deal with our polarized neutron data[10] and ab initio theoretical calculations.[11]

It is usual in charge-density studies to discuss the results using Fourier maps, showing the difference between the observed density and that of a suitable reference state. More recently, in connection with transition-metal complexes, it has become the practice to employ least-squares fitting of 3d electron populations on the metal

(1) Figgis, B. N.; Forsyth, J. B.; Mason, R.; Williams, G. A. *J. Chem. Soc.* **1981**, 1837-1845.
(2) (a) Figgis, B. N.; Reynolds, P. A.; Williams, G. A. *J. Chem. Soc., Dalton Trans.* **1980**, 2339-2347. (b) Chandler, G. S.; Figgis, B. N.; Phillips, R. A.; Reynolds, P. A., Mason, R.; Williams, G. A. *Proc. R. Soc. Lond, Ser. A.*, in press.
(3) Rees, B.; Mitschler, A. *J. Am. Chem. Soc.* **1976**, *98*, 7918-1924.
(4) Stevens, E. D.; Delucia, M. L.; Coppens, P. *Inorg. Chem.* **1980**, *19*, 813-820.
(5) Iwata, M. *Acta. Crystallogr., Sect. B* **1977**, *B33*, 59-69.
(6) Porai-Koshits, M. A.; Dikareva, L. M. *Sov. Phys. Crystallogr. (Engl. Transl.)* **1960**, *4*, 611-616.
(7) Figgis, B. N.; Reynolds, P. A.; White, A. H.; Williams, G. A.; Wright, S. *J. Chem. Soc., Dalton Trans.* **1981**, 997-1003.
(8) Figgis, B. N.; Kennedy, B. J.; Murray, K. S.; Reynolds, P. A.; Wright, S. *Aust. J. Chem.* **1982**, *35*, 1807-1813.
(9) Figgis, B. N.; Reynolds, P. A.; Williams, G. A.; Lehner, N. *Aust. J. Chem.* **1981**, *34*, 993-999.
(10) Figgis, B. N.; Mason, R.; Reynolds, P. A. *J. Am. Chem. Soc.* **1982**, *104* (following paper in this issue).
(11) Chandler, G. S.; Phillips, R. A., unpublished data.

0002-7863/83/1505-0434$01.50/0

atom,[3-5] As a suitable reference state, in addition to the usual superposition of spherical atoms, we intend to use a state derived from the data by least-squares fitting of a chemically reasonable model which employs a more complete set of valence electrons, This set will be 3d and 4p on the nickel atom and appropriate sp hybrids on the other atoms. In polarized neutron studies this procedure is necessary since, for experimental reasons, the data set cannot be even nearly complete.[12] Serious errors can be introduced into the corresponding Fourier maps by the "holes" in the data. For the X-ray data the procedure provides numerical estimates of such qualitative concepts as "π back-bonding", etc. The disadvantage of such model fitting is that it can lead to errors in interpretation, since no model is a unique fit to a data set. In particular, terms not included in the model, such as overlap density, can be projected into the valence density. However, if we are conservative in the number and chemical reasonableness of the valence functions fitted—in other words, we fit only low-order multipoles—then the overlap terms will remain relatively unchanged as they are known to project relatively inefficiently.[13,14] The Fourier difference map between observation and this model will show more clearly the overlap terms and other density of "unknown origin", since the effects of atomic hybridization, which are thought to be known, will have been removed. This approach also has the advantage of allowing a unified discussion of, and link between, the X-ray, polarized neutron, and theoretical results, This is discussed further in Figgis et al.[2b]

Experimental Section

The compound *trans*-$[Ni(NH_3)_4NO_2)_2]$ was prepared by a standard method.[15] A prismatic crystal suitable for X-ray diffraction measurements was obtained by cleavage of a twinned crystal along the (001) twinning plane. It was then coated with a thin layer of Canada balsam to minimize decomposition.

X-ray Data Collection. After initial photography the crystal was mounted on a Syntex $P2_1$ four-circle diffractometer equipped with a graphite single-crystal monochromator and a Syntex LT-1 low-temperature attachment. The cell constants at approximately 110 K were determined by a least-squares refinement of the 24 diffractometer setting angles of 6 reflections. A complete sphere of data was collected out to a 2θ maximum of 100°. Six standard reflections were measured every 100 reflections, and recentered every 200 reflections. The experimental peak width (in the ω–2θ mode) corresponded to the instrumental resolution (ca. 0.7° at low values of 2θ), indicating a crystal mosaic spread less than that. Even so, a generous scan width (2.6° + $\alpha_1\alpha_2$ splitting) was employed. There was a 5% decrease in intensities, uniform over the six standards, over the data collection period, reflecting some crystal decomposition. Equivalent reflections were collected at very different periods over the data measurement program, since cycling over *hkl* took place and data was not collected in shells corresponding to ranges of 2θ. The periodic recentering showed cell changes corresponding to a maximum temperature excursion of 4 K. The absolute value of the temperature 110 K is known only to a precision of 10 K. Crystal and experimental data are given in Table I.

Data Processing. After correction of the measured intensities by the use of the monotonically decreasing standard intensities, the data were corrected analytically for absorption with program ABSCOR of the XRAY 76 system.[16] After correction the agreement factor between equivalents, R_I ($=\sum Av[I - Av(I)]/\sum Av(I)$), was 0.020. This value gives an assessment of the efficiency of the absorption and decay corrections. It was noticed that around two particular sets of diffractometer angles the intensities of reflections were up to 10% less than their equivalent reflections intensities. This was found to correspond to shading of the beam by the mounting fiber. About 20 individual, shaded equivalents were accordingly removed before averaging the equivalents to give the final set of 2150 unique reflections. The standard deviation of the mean intensity was estimated from the variance between equivalents as described in ref 17.

Table I. Crystal Data and Experimental Conditions

cryst dimensns	(010) to (0$\bar{1}$0) 0.21 mm (001) to (00$\bar{1}$) 0.32 (100) to ($\bar{1}$00) 0.25
space group	$C2/m$, $Z = 2$
unit cell at 110 (10) K	
	a = 1061.7 (4), b = 681.2 (2), c = 590.6 (3) pm β = 114.83 (3)°, V = 0.3876 nm^3 ρ(X-ray) = 1.875 Mg m^{-3} for 110 K
radiation	Mo Kα ($\bar{\lambda}$ = 71.069 pm)
monochromator	graphite plate, (002)
scan mode, rate	$\omega/2\theta$, variable
scan width	2.6° + $\alpha_1\alpha_2$ splitting
background counting time	0.5 of scan time
no. of measured reflctns	6514
no. of unique reflctns	2109
$(\sin\theta_{max})/\lambda$	10.8 nm^{-1}
μ(Mo Kα)	2.48 mm^{-1}
transmission factor	0.551–0.648

Least-Squares Refinements. Spherical Atom Refinements. The initial positional coordinates used were those previously reported.[7] Least-squares refinement of atomic coordinates and anisotropic thermal parameters (for atoms other than H) was performed by use of program CRYSLQ from the X-RAY 76 program system[16] in the full-matrix mode. The function $\sum\omega[I_{obsd} - I_{calc}]^2$ was minimized, where $\omega = 1/(\sigma^2(I))$. No data were rejected. Neutral atom scattering factors were taken from ref 18, except for hydrogen where ref 19 was used, and were modified (apart from hydrogen) for anomalous dispersion.[20] Three refinements were made with the full data set (refinement I), a low-angle set (refinement II), and high-angle set (refinement III). Discrepancy indices etc. are given in Table II, while atomic parameters are given in Table III. Hydrogen parameters in refinement III were fixed at the values obtained in refinement II. In refinement I no correlation coefficient between any hydrogen parameter and any non-hydrogen parameter exceeded 0.25. Thus, the fixing of the hydrogen parameters will have a negligible effect on the rest. Refinements II and III were restricted in $(\sin\theta)/\lambda$ so that the ranges did not abut. This was done so as to maximize any differential effects due to anharmonicity of thermal vibrations, thermal diffuse scattering, etc. between them and thus to make any such systematic effects more obvious. Addition of a refineable extinction parameter gave a small negative value not significantly different from zero, showing that extinction was negligible; examination of the data showed no evidence for anisotropic extinction in any sector of reciprocal space.

The present results are consistent with the molecular geometry as determined by neutrons and X-rays and extensively discussed elsewhere,[7,9] together with an illustration of the molecular geometry.[7]

The thermal parameters are intermediate between those at 4.2[9] and 295 K[7] as expected. The thermal parameters from the high-angle refinement (III) are about 5% less than those from the low-angle refinement (II). If we except those for N(1), the ratio of high- to low-angle parameters ranges from 0.89 to 1.04. For N(1) the range is 0.74 to 1.22. The larger low-angle thermal parameters are expected, since the effect of valence electrons is to increase the apparent thermal parameters at low angles. It is apparent that the valence distribution around N(1) is *not* well described by a spherical atom refinement.

Although significant valence effects, of lone pairs for example, extend past 8.5 nm^{-1} in reciprocal space, the bulk of their effect is at lower angles.[21] The high-angle refinement may then be taken as an estimate of the atomic thermal motion. The accuracy of the parameters is limited by thermal diffuse scattering, anharmonicity, and valence effects. The difference between high- and low-angle refinements suggests that complete elimination of valence effects from the high-angle data could decrease the thermal parameters by less than a further 5%. Thermal diffuse scattering is well-known to produce an apparent decrease in thermal parameters.[22] Therefore, use of high-angle thermal parameters to interpret low-angle data for valence effects is reasonable since TDS affects both in the same way. Refinement of the data in shells of reciprocal

(12) Figgis, B. N.; Reynolds, P. A.; Williams, G. A.; Mason, R.; Smith, A. R. P.; Varghese, J. N. *J. Chem. Soc., Dalton Trans.* **1980**, 2333–2338.
(13) Newton, M. D. *J. Chem. Phys.* **1969**, *51*, 3917–3926.
(14) Wedgwood, F. A. *Proc. R. Soc. London A Ser.* **1976**, *349*, 447–465.
(15) Soret, L.; Robineau, F. *Bull. Soc. Chim. Fr.* **1889**, *2*, 138–139.
(16) Stewart, J. M. The Computer Science Center, University of Maryland, College Park, MD, The XRAY System-Version of 1976, Technical Report TR-446.
(17) Reynolds, P. A.; Figgis, B. N.; White, A. H. *Acta Crystallogr.* **1981**, *37*, 508–513.
(18) Cromer, D. T.; Mann, J. B. *Acta Crystallogr., Sect A* **1968**, *A24*, 321–324.
(19) Stewart, R. F.; Davidson, E. R.; Simpson, W. T. *J. Chem. Phys.* **1965**, *42*, 3175–3187.
(20) Cromer, D. T.; Liberman, D. *J. Chem. Phys.* **1970**, *53*, 1891–1898.
(21) Coppens, P. *Top. Curr. Phys.* **1978**, *6*, 71–111.
(22) Willis, B. T. M.; Pryor, A. W. "Thermal Vibrations in Crystallography"; Cambridge University Press: Cambridge, 1975; pp 232–239.

Table II. Refinement Results

	refinement			
	I	II	III	IV (valence)
$(\sin\theta)/\lambda$ range, nm^{-1}	0–10.8	0–7.0	8.5–10.8	0–8.5
N_{obsd}	2109	590	1061	1048
N_{var}	45	45	33	37
$R(F) = \Sigma\|\|F_o\| - \|F_c\|\|/\Sigma\|F_o\|$	0.023	0.016	0.034	0.017
$R_w(I) = [\Sigma\omega(I_o - I_c)^2/\Sigma\omega I_o^2]^{1/2}$	0.035	0.029	0.055	0.031
$\chi = [\Sigma\omega(I_o - I_c)^2/(N_{obsd} - N_{var})]^{1/2}$	2.1	2.8	1.51	2.36
scale factor	12.60 (1)	12.63 (3)	12.69 (10)	11.77 (10)

Table III. Relative Coordinates (×10⁵) and Thermal Motion Parameters (pm^2), Given by $T = \exp(-2\pi^2\Sigma_i\Sigma_j U_{ij}h_i a_i^* h_j a_j^*)$

	x/a	y/b	z/c	U_{11}	U_{22}	U_{33}	U_{12}	U_{13}	U_{23}
Ni I	0	0	0	68 (1)	91 (1)	100 (1)	0	49 (1)	0
II	0	0	0	71 (2)	92 (1)	106 (1)	0	53 (1)	0
III	0	0	0	69 (1)	90 (1)	98 (1)	0	48 (1)	0
N(1) I	20 028 (7)	0	−632 (12)	95 (2)	119 (2)	130 (2)	0	64 (2)	0
II	20 007 (13)	0	−613 (24)	117 (6)	105 (5)	150 (6)	0	77 (5)	0
III	20 049 (9)	0	−642 (20)	87 (2)	129 (3)	119 (3)	0	57 (2)	0
N(2) I	6555 (5)	22 357 (8)	27 148 (9)	116 (2)	142 (2)	149 (2)	−11 (1)	69 (1)	−25 (1)
II	6553 (9)	22 336 (15)	27 131 (17)	117 (4)	145 (4)	153 (4)	−9 (3)	70 (3)	−19 (3)
III	6553 (8)	22 375 (12)	27 172 (16)	116 (2)	141 (2)	146 (2)	−13 (1)	67 (1)	−29 (1)
O(1) I	30 842 (6)	0	19 011 (12)	94 (2)	251 (3)	170 (2)	0	34 (2)	0
II	30 846 (11)	0	19 001 (21)	101 (5)	255 (6)	174 (5)	0	37 (4)	0
III	20 823 (11)	0	19 003 (28)	95 (3)	243 (5)	176 (4)	0	37 (3)	0
O(2) I	21 318 (7)	0	−20 910 (12)	161 (2)	208 (2)	167 (2)	0	118 (2)	0
II	21 320 (12)	0	−20 915 (20)	171 (6)	205 (6)	178 (5)	0	128 (5)	0
III	21 339 (12)	0	−20 822 (26)	152 (3)	213 (4)	161 (3)	0	109 (3)	0
H(1) I	9992 (109)	17 940 (246)	42 231 (206)	304 (30)					
II	10 019 (152)	17 994 (341)	42 368 (295)	288 (45)					
III	10 019 (152)	17 994 (341)	42 368 (295)	288 (45)					
H(2) I	12 527 (109)	30 424 (217)	24 326 (196)	246 (29)					
II	12 602 (157)	30 309 (313)	24 422 (280)	262 (42)					
III	12 602 (157)	30 309 (313)	24 422 (280)	262 (42)					
H(3) I	−734 (116)	30 108 (188)	24 706 (192)	239 (28)					
II	−760 (166)	30 059 (267)	24 773 (271)	240 (41)					
III	−760 (166)	30 059 (267)	24 773 (271)	240 (41)					

space, which for Cs_3COCl_5 was a sensitive indicator of anharmonicity,[17] showed no effects at higher values of $(\sin\theta)/\lambda$ (8.5 to 10.8 nm^{-1}). We conclude that use of the high-angle data will introduce errors equivalent to less than a 5% error in the thermal parameters. Since the thermal parameters and the scale factor are correlated, we may expect an error of up to ~5% in the scale factor.

Valence or Aspherical Atom Refinements. Theory. We can write the static electron density, ρ, in the Hartree–Fock approximation, as a sum of one-electron molecular orbitals (i), atomic orbitals ϕ_k^{nlm} with the usual quantum numbers nlm centered on the kth atom, and MO coefficients C_{nlm}^{ik}.

$$\rho = \sum_i \sum_{k,k'} \sum_{\substack{nlm \\ n'l'm'}} C_{nlm}^{ik} C_{n'l'm}^{ik'} \phi_k^{nlm} \phi_{k'}^{n'l'm'}$$

We then neglect all overlap between atomic functions on different atoms and we separate out a "core" electron density, which corresponds to MO's essentially localized on a single atom. The Fourier transform of this may be written,[23,24] using standard procedures,[25] in terms of Clebsch–Gordon (or 3 - j) symbols, separating angular and radial terms,

$$F(\kappa) = F_{core}(\kappa) + \sum_{\substack{l,k \\ nlm \\ n'l'm'}} C_{nlm}^{k} C_{n'l'm'}^{k} \sum_{m''=0}^{\infty} [(8m'' + 4)\pi]^{1/2} (i^{m''}) \times \langle j_{m''}(|\kappa|)\rangle_{nl,n'l'} C^{m''}(lm,l'm') Y_{m''}^{l-l'}(\phi,\theta)$$

where κ is the scattering vector, $C^{m''}(lm,l'm')$ the 3- j symbol, $Y_{m''}^{l-l'}(\phi,\theta)$ a spherical harmonic function, and $\langle j_{m''}(|\kappa|)\rangle_{nl,n'l'}$ is defined by

$$\langle j_{m''}(|\kappa|)\rangle_{nl,n'l'} = \int r^2 P_{nl}(r) P_{n'l'}(r) j_{m''}(|\kappa|r)\, dr$$

$P_{nl}(r)$ is the radial part of the atomic orbital ϕ_k^{nlm} and $j_{m''}(|\kappa|r)$ is the spherical Bessel function of order m''. Explicit expressions for $l = l' = 0, 1$;[26] $l = l' = 2, 3$;[23] and $l = 0$; $l' = 1$[27] have been given previously. We have used throughout the spherical harmonic and atomic orbital conventions and definitions of Condon and Shortley.[25] For a complete set of atomic functions with refinement of Cartesian axis direction, this method is equivalent to a complete multipole expansion. *The use of a restricted set of atomic functions is equivalent to a restricted multipole expansion in which the terms neglected are not cut off at an arbitrary order of multipole but chosen on the basis of chemical intuition.* This method has the advantage of providing an initial estimate for the radial part of the form factors, $\langle j_{m''}(|\kappa|)\rangle_{nl,n'l'}$. The connection between multipole expansions and orbital products for pp and dd products has been published.[28,29]

This approach rests on a number of theoretical assumptions, in particular that the effects of configuration interaction are not important. If these latter are important, then the coefficients and the quantities $\langle j_{m''}(|\kappa|)\rangle$ have no direct theoretical meaning and become merely coefficients and radial dependencies of a restricted multipole expansion. In some cases this may be seen by the unphysical values adopted by the "atomic population" and "atomic radial" parameters. It is possible to include many higher multipoles: For example, in oxalic acid multipoles up to order 4[30] have been employed. In such a case it is possible to project much of the two-center density into these one-center terms.[13] If, however, we restrict ourselves to a minimal, chemically reasonable basis set, e.g., sp hybrids on N and O, then the two-center terms are projected relatively inefficiently into these low-order multipoles.[13,14] Any residual electron density then is likely to be due to either two-center overlap terms or inadequacies in the one-center atomic basis used in the modeling.

If the scale factor is correct, summation of the population parameters and the integrated residual density must give the total valence population

(23) Weiss, R. J.; Freeman, A. J. *Phys. Chem. Solids* **1959**, *10*, 147–161.
(24) "International Tables for X-ray Crystallography"; Kynoch Press: Birmingham, 1974; Vol. IV, pp 102–147.
(25) Condon, E. V.; Shortley, G. H. "The Theory of Atomic Spectra"; Cambridge University Press: Cambridge, 1957; pp 158–186.
(26) McWeeney, R. *Acta Crsytallogr.* **1951**, *4*, 513–519.
(27) Dawson, B. *Acta Crystallogr.* **1960**, *13*, 403–408.
(28) Stevens, E. D.; Coppens, P. *Acta Crystallogr., Sect. A* **1979**, *A35*, 536–539.
(29) Varghese, J. N.; Mason, R. *Proc. R. Soc. London, Ser. A* **1980**, *372A*, 1–7.
(30) Dam, J.; Harkema, S.; Feil, D. *Acta Crystallogr., Sect. B* **1980**, *B36*, 1864–1875.

of electrons, 76 per molecule. Since the scale factor is uncertain to about 5%, we may expect a corresponding error in our estimate of valence populations. This can be reduced in two ways. If the model for the electron density is thought to be complete, a crystal electroneutrality constraint can be incorporated in the least-squares process. This procedure may be dangerous, since if diffuse valence functions are included they have little effect on the goodness-of-fit but a large effect on electron populations. The net result may be that the scale factor may *remain* incorrect, caused by, for example, the "soaking up" of high-angle errors such as TDS. Meanwhile the electroneutrality condition merely changes the diffuse valence function values, and hence "atomic charges", to physically unreal values. A safer procedure is to take the high-angle thermal parameters and use these unchanged in the low-angle refinement. Since the $(\sin\theta)/\lambda$ is small, the errors introduced will be small. The scale factor should then be regarded as a refineable parameter in the low-angle refinement. The result will be a "low-angle" scale factor and a "high-angle" scale factor. Differences between these two factors may be indicative of small errors in the "high-angle" scale factor, i.e., in the values of the *thermal parameters*.

Application to $Ni(NH_3)_4(NO_2)_2$. We use program ASRED,[2] which has already been extensively employed to analyze spin-density data in terms of "atomic orbital populations"—more accurately multipole coefficients. The radial integral incorporates a refineable radial $K^{nln'l'}$ defined by $\langle j_{m'}(K^{nln'l'}|\kappa|)\rangle_{nl,n'l'}$. An increase in $K^{nln'l'}$ above unity reflects an expansion of the total valence density on atom k from the starting value, which is calculated from Hartree–Fock atomic theory.[24] The "atomic orbital populations" refined in the present treatment were five 3d orbitals and three 4p on Ni, four sp^3 hybrids on N(2), a ls population on each H, a p_π orbital on N(1), O(1), and O(2), three sp^2 σ-bonding hybrids on N(1), and two sp hybrids oriented along the N–O bonds and a p orbital in the NO_2 plane for O(1) and O(2). Each of N(1), N(2), O(1) and O(2) have four sp hybrids chosen so as to reflect symmetry in the local environment. No 4s orbital was used in the basis set on the nickel atom since it would be very highly correlated with the 4p populations, due to their similar radial extents. In the subsequent results, if we were to postulate a 4s population of C, then given $4p_x$, $4p_y$, and $4p_z$ populations each reduced by C/3, the fit to the model would be indistinguishable. We should note, however, that (a) C could not be arbitrarily large, since then 4p population would become negative, and (b) anisotropy in the 4p populations would not be reduced by the presence of 4s.

These orbitals are listed in Table IVA. The d orbitals on the nickel atom are labeled according to Cartesian axis system appropriate to the molecular point group, that is, $x\|b$, $y\|c^*$, $z\|a$. Note that this is not the "natural" octahedral system, and our axis system gives d_{xy} and d_{z^2} not $d_{x^2-y^2}$ and d_{z^2} as the octahedral e_g set. The 3d and 4p radial factors on Ni were calculated from a Ni^+ ($\cdots 3d^8 4p^1$) atomic calculation,[31] those of N, O, H from ref 24.

The atomic positional and thermal parameters used were those of the high-angle refinement (III), since this provides the best estimate of these quantities and is less biased by valence effects than is the low-angle data. The scale factor was included as a refineable parameter. The results of the refinement are given in Table II and the values derived for the parameters in Table IVB. Use of the complete data set and refinement of all position, thermal, and population parameters together will only give a more reliable estimate of populations if the model is complete (i.e., $\chi \sim 1.0$). Since this is not so, the use of high-angle data to determine atomic position and thermal parameters, which are not varied in refinements using the rest of the data (low-angle), provides the best method of estimating valence effects. All the 45 independent correlation coefficients were less than 0.67, with all but 4 less than 0.3. The scale factors of the high- and low-angle refinements differ by 6.6%, reflecting the estimated thermal parameter error of ~5%. In order to save computation, the radii of both nitrogen atoms and of both oxygen atoms were set equal, respectively, even though the atoms are not crystallographically and/or chemically equivalent. Subsequent relaxation of this requirement, allowing all N and O parameters to vary, produced no significant changes.

Fourier difference maps of the valence refinements in the *ac* plane, which contain Ni, N(1), O(1), and O(2) (nickel–nitro), and the *bc** plane, containing N(1), N(2), and H(1) (nickel–ammine) are shown in Figure 1C and 1D. Corresponding results for a spherical atom refinement are shown in Figure 1A and 1B. Increase of the limit of integration to 10.8 nm^{-1} produces qualitatively similar maps, except that peak and trough heights around the nickel atom are increased. An underestimate of true 3d orbital densities due to series termination errors is well-known.[21,32]

(31) Stevens, E. J.; Figgis, B. N., personal communication.
(32) Ohba, S.; Toriumi, K.; Sato, Saito, *Acta Crystallogr., Sect. B* **1978**, *B34*, 3535–3542.

Table IV

A. Orbitals Used in Valence Refinement and Their Alignment

atom	description	θ	ϕ[a]
Ni	$3d_{xy}$		
	$3d_{yz}$		
	$3d_{xz}$ 3d set		
	$3d_{z^2}$		
	$3d_{x^2-y^2}$		
	$4p_x$		
	$4p_y$ diffuse 4p		
	$4p_z$		
N(2)	$sp^3(1)$ 2s2p, sp^3 hybrids	90	45
	$sp^3(2)$ (1)$\|\|N(2)$-Ni,[b] (2)$\|\|N(2)$-H(1)	90	117
	$sp^3(3)$ (3)$\|\|N(2)$-H(3), (4)$\|\|N(2)$-H(2)	155	−9
	$sp^3(4)$	46	−9
H(1)	1s		
H(2)	1s hydrogen 1s orbitals		
H(3)	1s		
N(1)	$sp^2(1)$ 2s2p, sp^2 hybrids	0	0
	$sp^2(2)$ (1) $\|\|N(1)$-Ni; (2)$\|\|Ni$-O(2)	59	90
	$sp^2(3)$ (3) $\|\|N(1)$-O(1)	59	−90
	p_π 2p orbitals, ⊥ Ni-NO_2 plane	90	0
O(1)	sp(1) 2s2p sp hybrids both $\|\|O(1)$-N(1)	121	90
	sp(2) (1) lobe points toward N(1)	59	90
	$p_\pi(1)$ 2p orbitals, (1) is ⊥ $NiNO_2$ plane	90	0
	$p_\pi(2)$ (2) is in NO_2 plane, ⊥ Ni-O(1)	31	90
O(2)	sp(1) 2s2p hybrids both $\|\|$ O(2)-N(1)	121	90
	sp(2) (1) lobe points toward N(1)	59	90
	$p_\pi(1)$ 2p orbitals (1) is ⊥ $NiNO_2$ plane	90	0
	$p_\pi(2)$ (2) is in NO_2 plane, ⊥ N(1)-O(2)	31	90

B. Valence Refinement Parameters[c,d]

nickel		H(1)	
$3d_{xy}$	1.28 (7)	1s	0.77 (4)
$3d_{yz}$	1.80 (6)	H(2)	
$3d_{xz}$	1.31 (6)	1s	0.92 (3)
$3d_{z^2}$	1.36 (8)	H(3)	
$3d_{x^2-y^2}$	1.84 (7)	1s	0.93 (3)
radius 3d (κ^{3d3d})	1.013 (6)	O(1)	
$4p_x$	1.59 (20)	sp(1)	1.43 (3)
$4p_y$	0.09 (20)	sp(2)	1.62 (3)
$4p_z$	−0.19 (20)	$p_\pi(1)$	1.61 (4)
radius 4p (κ^{4p4p})	0.95 (1)	$p_\pi(2)$	1.61 (4)
N(1)		radius	1.046 (4)
$sp^3(1)$	1.59 (3)	O(2)	
$sp^3(2)$	1.21 (3)	sp(1)	1.42 (3)
$sp^3(3)$	1.21 (3)	sp(2)	1.64 (3)
$sp^3(4)$	1.24 (2)	$p_\pi(1)$	1.43 (4)
radius	1.052 (5)	$p_\pi(2)$	1.74 (4)
N(2)		radius	1.046 (4)
$sp^2(1)$	1.66 (4)		
$sp^2(2)$	1.32 (4)		
$sp^2(3)$	1.26 (4)		
p_π	0.86 (4)		
radius	1.052 (5)		

[a] θ and ϕ are the approximate polar angles of the direction of the positive lobe (where applicable) of non-nickel atoms relative to the nickel Cartesian axis system. $Z\|\|Ni$-N(1); $X\|\|$(Ni-N(1) × N(1)-O(2)); $Y\|\|z \times X \simeq \|\|$O(1)-O(2). [b] Notation X-Y represents the vector joining atoms X and Y. [c] Population, units of electrons; radial parameters ($\kappa^{nln'l'}$) for all 21,21' are set identical for N(1), N(2); O(1), O(2). [d] Total residue from difference map = 0.27 (13).

Results

Deformation Electron Density after Subtraction of Spherical Atoms. Around the Nickel Atom. The crystal-field model of the Ni^{2+} ion in a tetragonal field with small distortion from octahedral symmetry gives orbital populations (in the D_{2h} coordinate system) $d_{xy}^1 d_{yz}^2 d_{xz}^2 d_{z^2}^1 d_{x^2-y^2}^2$. This should give rise to holes in the residual electron density along the six Ni–N bond directions at ~50 pm from the nickel atom and peaks directed into the faces of the octahedron. In other octahedral complexes these crystal-field predictions are observed.[3,4,32] We also observe such a distribution. There is a hole of −500 (−800) electron nm^{-3} at 50 pm along the Ni–NO_2 bond from the nickel atom and −200 (−450) at 55 pm

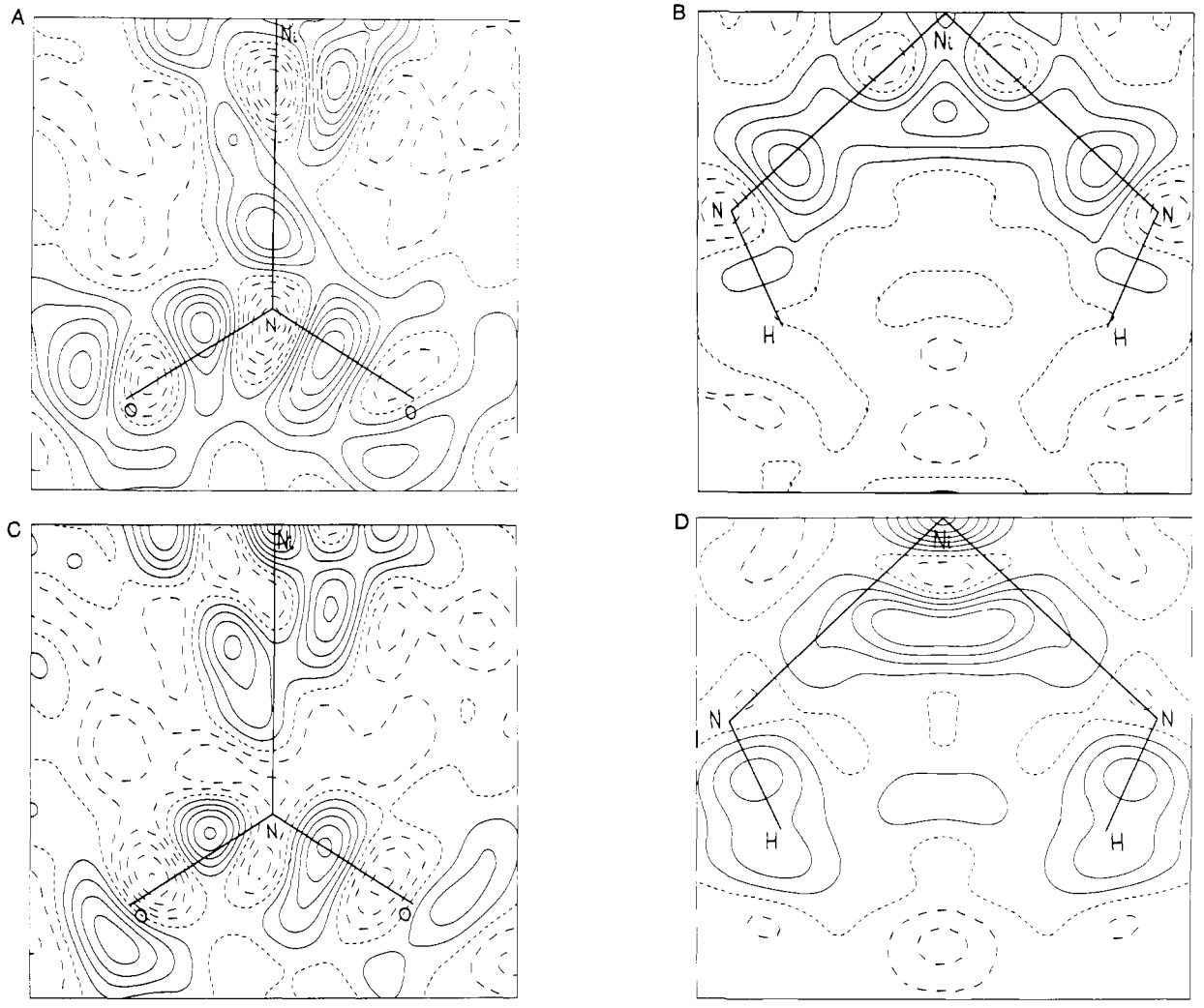

Figure 1. (A) Section through nickel–nitro group plane showing the deformation density resulting from the difference between observed and spherical-atom model structure factors. Contour interval 100 electron nm^{-3}; positive if solid, negative if dashed, zero if dotted. (B) Section through nickel–ammine group (containing N(2) and H(1)) showing the deformation density resulting from the difference between observed and spherical-atom model structure factors. Contours as in Figure 1a. (C) Section through nickel–nitro group plane showing the residual density resulting from the difference between observed and aspherical valence-model refinement structure factors. (D) Section through the nickel–ammine group (containing N(2) and H(1)) showing the residual density resulting from the difference between observed and aspherical valence-model refinement structure factors. Contours as in Figure 1a.

along the $Ni–NH_3$ bond. Figures in brackets refer to difference maps with a 10.8 nm^{-1} limit of integration, The peaks in the faces of the octahedron are less clear, +600 (1300) electron nm^{-3} at 55 pm and +200 (400) in the $Ni(NO_2)_2$ plane and 0 (0) perpendicular to it. This "3d" distribution is markedly nontetragonal with the d_{yz} population much greater than d_{xz}. There is a further diffuse feature of 450 (450) electron nm^{-3} at 70 pm from the nickel atom along c^*, in the $Ni(NO_2)_2$ plane. This is an ellipsoid of density, elongated along b, The simple tetragonal crystal-field model is therefore not adequate—the density is neither tetragonal nor entirely of 3d symmetry. All other features on the map are little changed on increase of the limit of integration of 7.0 to 10.8 nm^{-1} so that we will henceforth quote only the former.

Around the Ammonia Fragment. We observe only a peak of 460 electron nm^{-3} at 55 pm from the nitrogen atom along the Ni–N axis. This is the ammonia lone pair, as also observed in $Co(NH_3)_6Cr(CN)_6$.[5] The lack of features in the N–H bond arises because in the X–X method the hydrogen positions are refined from low-angle data; their position is shifted toward the nitrogen from the true nuclear position as determined by neutron diffraction.[9] This shift of electron density into the N–H bond is a well-known effect.[33] The N–H(1) bond possesses an apparently higher isotropic thermal motion than either N–H(2) or N–H(3), which may indicate a difference in bonding.

Around the Nitrite Ion. If the interpretation of Ohba et al. that the main features in the difference map are associated with the free nitrite ion rather than bonding to the metal is correct, we may expect to see similar features to those in $K_2Na[Co(NO_2)_6]$.[32] Our difference map does closely resemble theirs. we observe a peak of 500 electron nm^{-3} at 50 pm from the nitrogen atom on the Ni–N axis, which is assigned to a "lone pair" on the nitrogen. There are two troughs of −500 electron nm^{-3} 40 pm above and below the nitrogen atom (i.e., parallel to b). Both these features are expected from a nitrogen hybridized $[sp^2(1)]^2[sp^2(2)]^1[sp^2(3)]^1[p_\pi]^1$. In addition there are peaks 500 electron nm^{-3} at 50 pm from the nitrogen atom and troughs −500 electron nm^{-3} 30 pm from each oxygen atom along each N–O bond. In addition at 45 pm from each oxygen atom there are probably 4 peaks of 100–600 electron nm^{-3}, The peak–O–peak angle is about 130°. These may be assigned as oxygen "lone pairs". Ohba et al.[32] observed peaks of π symmetry in the overlap region of the N–O bond which we do not see, The general arrangement of peaks, troughs, and lone pairs in the N–O bond resembles those in the same bonds in *p*-nitropyridine *N*-oxide[34] and even in the C–O bond

(33) Olovsson, I.; Jonsson, P. G. "The Hydrogen Bond"; Schuster, P., Zundel, G., Sandorfy, C., Eds.; North Holland: Amsterdam, 1976; Vol. 2, pp 393–457.

(34) Coppens, P.; Lehmann, M. S. *Acta Crystallogr.; Sect. B* **1977**, *B32*, 1777–1784. Wang, Y.; Blessing, R. H. Ross, F. K.; Coppens, P. *Ibid.* **1976**, *B32*, 572–578.

of cyanuric acid[35] and oxalic acid dihydrate,[30] as well as $K_2Na[Co(NO_2)_6]$.[32]

Specific Metal–Ligand Bonding Effects. Apart from the area around the nickel atom itself, specific effects of metal–ligand bonding do not seem to be obvious. A more quantitative assessment of electron density and orbital populations on the ammonia and nitrite ligands is therefore required.

Aspherical Atom Refinements and Residual Difference Density. The aspherical hydridized atom refinement outlined earlier (vide supra) can give more quantitative information on atomic hybridization and electron populations. The refined values of the "orbital populations" and radial parameters are given in Table IV. In the Fourier difference maps we observe three features. Firstly, around the nickel atom there remains "diffuse" density. Secondly, there is density of d_{yz} symmetry at 80 pm from the nickel atom and of peak height 500 electron nm^{-3}. Thirdly, there is an ellipsoid of density elongated along *b* and of peak height 400 electron nm^{-3} at 80 pm from the nickel atom in the c^* direction. Both the later features are of shape and angular extent incompatible with 4s or 4p functions. The integrated density involved is 0.12 (5) electron.

On the nitrite ion there remains along each N–O bond a positive peak, a trough, and a small positive peak behind the oxygen atom, all of σ symmetry. They give a total net excess electron density of 0.02 (2) in each N–O bond, The first two features are too localized to be fitted by relatively diffuse 2s2p valence hybrids on N and O atoms and may come from two-center density. The small positive peak behind the oxygen atom is a residue from the "lone-pair" peaks on that atom. We use an sp hybridized oxygen to model the valence density. If we use sp^2 hybridized oxygen we obtain a trough here. Therefore, the oxygen "lone pairs" in the NO_2 planes are intermediate in hybridization between sp and sp^2.

On the ammonia molecule there has now appeared a density (300 electron nm^{-3}) midway along the N–H(1) bond with a population 0.019 (5) electron. This is associated with a fall in the H(1) "1s" population from 1.0 to 0.8. The "1s" populations of H(2) and H(3) remain close to 1.0. The bonding density in the N–H(1) bond is no longer well described by a simple spherical "1s" H density.[19] In the N–H(1) bond relative both to N–H(2) and N–H(3), and H_2,[19] there has been a migration of charge along the bond from the "normal" position of the centroid of charge closer to the nitrogen atom giving a marked charge asphericity which a spherical H "1st" can no longer accommodate by a simple shift in its center toward the nitrogen atom.

To discuss the chemical significance of these results, we combine the features in the difference maps with the valence populations.

Discussion

Charge Transfers. From the data in Table IV we can see that each ammonia ligand has a net charge of +0.11 (6) and each nitrite anion of −0.62 (8) electron. thus there has been a net migration onto the Ni^{2+} of 1,20 electron leaving the nickel atom with a net charge of +0.80 (10).

Nitrite Anion. If we further break down the 0.38 electron lost from each NO_2^- anion we find that the π electron system contains 3.89 (6) and the σ system 13.73 (6) electron in the valence shell. Therefore, in each nitrite ligand the π system has donated 0.11 (6) electron and the σ system 0.27 (6) electron to the Ni^{2+} ion. As expected, therefore, in the nitrite ligand σ-bonding effects are much greater than π bonding; indeed π bonding is nonzero only at an 80% confidence level. We can compare our "atomic populations" with those from a Mulliken analysis of theoretical wave functions. We should note that the ~5% expansion of the valence shells is probably an indication that we are partitioning two-center, overlap densities between the N and O atoms, and so the comparison with theory is not exact even if we neglect the effect of the metal atom. In Table V we compare our experiments with single- and double-ζ quality RHF calculations[36] and the results of a simple atomic hybridization scheme.

Table V. Valence Population in the Nitrite Anion

	theory			
	single ζ	double ζ	hybridizatn	expt
O σ	5.0	4.96	5	4.73 (6)
π	1.56	1.49	1.5	1.52 (9)
N σ	3.96	4.08	4	4.24 (6)
π	0.88	1.01	1	0.86 (4)
net O charge	−0.56	−0.35	−0.5	−0.25 (10)
net N charge	+0.16	−0.09	0	−0.12 (6)
overlap density σ	0.01	0.35	0	
π	0.25	0.19	0	

The theoretical calculations agree in broad outline with the simple hybridizaiton treatment. When we compare with experiment, the major discrepancy is in the oxygen σ populations. This might indicate that the *net* effect of the metal–ligand bonding is to transfer electrons from the electronegative oxygen atoms, through the nitrogen atoms via the σ valence framework to the Ni^{2+} ion, This is precisely what we would predict from the principle that covalent bonding tends to reduce the charge differential between different parts of a molecule. If we examine the individual hybrid atomic orbital populations, the lone pairs predicted on the simplest theory [N, $sp^2(1)$; O, $sp(2) + p_\pi(2)$] do have greater populations (mean 1.65 (5)) than the rest, which this theory predicts as population 1 (the experimental mean is 1.36 (8)), The RHF predictions are not as clear-cut; the distinction between "lone pairs" and "bonding pairs" is no longer clear. The only theoretical treatment in which an electron density map for the NO_2^- ion has been published[32] is a CNDO/2 calculation which shows a good qualitative agreement, in peak shapes and positions, with our experimental difference density map.

Ammonia. In the ammonia ligand there is a net loss of 0.11 (6) electron to the Ni^{2+} ion, but a division of the contribution between N and H is not very meaningful due to the high overlap population (~1.2 electron /molecule[37]). We note that the amount of σ donation per ligand is $\sim^1/_3$ of that for the nitrite ion, a result expected, for example, on the basis of the spectrochemical series. The most interesting feature is the low H(1) electron "1s" population and its migration of charge toward N, relative to H(2) and H(3). We have previously observed in the infrared spectrum that one of the N–H bonds is anomalously weak,[7] and that fact presumably reflects the lack of electron density in the N–H(1) bond.

Nickel Atom. The nickel atom appears to have configuration $3d^{7.7(1)}$ (diffuse)$^{1.61(2)}$, giving a net charge of +0.8 (1). Thus more than the 1.2 electron donated by the σ-bonding ammonia and nitrite ligands ends up in diffuse metal orbitals. However, this does not occur directly as we can see from the d configuration $d_{xy}^{1.28(7)}d_{yz}^{1.80(6)}d_{xz}^{1.31(6)}d_{z^2}^{1.36(8)}d_{x^2-y^2}^{1.84(7)}$, which we can compare with the simple crystal-field theory result of $d_{xy}^1d_{yz}^2d_{xz}^2d_{z^2}^1d_{x^2-y^2}^2$. In ligand-field theory the effect of the σ bonding would be to change these populations to $d_{xy}^{1.44}d_{yz}^2d_{xz}^{2.22}d_{z^2}^{1.54}d_{x^2-y^2}^2$, if we employ the observed NH_3 and NO_2^- ligand charges. We note that the d_{xz} orbital theoretically donates electrons into the NO_2^- π system, whereas we observe a small transfer in the opposite direction from ligand π system to the metal atom. The σ-bonding populations are broadly comparable between experiment and ligand-field theory, the major discrepancy appearing only in the $3d_{xz}$ orbital. It appears that populations of that orbital is highly disfavored relative to the more diffuse $4p_x$ orbital. This causes the nickel environment to be markedly nontetragonal. Since $4p_y \sim 4p_z \sim 0$ it follows that $4s \sim 0$ also.

Simple crystal-field theory predicts on an electrostatic basis that $4p_x$ *is* the lowest in energy of the 4p orbitals. The position of the $3d_{xz}$ orbital depends on the relative sizes of octahedral,

(35) Coppens, P.; Vos, A. *Acta Crystallogr., Sect. B* **1971**, *B27*, 146–158. Verschoor, G. S.; Keulen, E. *Ibid.* **1971**, *B27*, 134–145.

(36) Petrolongo, C.; Scrocco, E.; Tomasi, J. *J. Chem. Phys.* **1968**, *48*, 407–411. Bonnacorsi, R.; Petrolongo, C.; Scrocco, E.; Tomasi, J. *Ibid.* **1968**, *48*, 1497–1508.

(37) Rauk, A.; Allen, L. C.; Clementi, E. *J. Chem. Phys.* **1970**, *52*, 4133–4144.

tetragonal, orthorhombic terms in the Hamiltonian, but it is not obviously the highest in energy, d_{z^2} being more likely. A simple explanation then of the *observed* configuration is that the transition $4p_x \leftarrow 3d_{xz}$ is of low energy, and a large CI component arising from the state produced by the single excitation $4p_x \leftarrow 3d_{xz}$ is included in the final nickel ground state.

Conclusion

The electron density in $Ni(NH_3)_4(NO_2)_2$, as measured by these X-ray diffraction experiments, shows features around the nickel atom due to both aspherical d-electron distribution and more diffuse electron density. The ligand electron densities are qualitatively similar to those measured in other metal ammines[5] and nitro complexes.[32]

A quantitative analysis of the electron density by means of an aspherical valence-shell refinement allows more quantitative conclusions to be drawn. These are in general accord with simple ligand-field theory. The electron distribution in the nitro group closely resembles calculations of that in the free nitrite anion, except that 0.38 (8) electron have been σ donated to the metal atom. The π system is much less affected by complexation. The ammonia molecule, as expected, is a much weaker σ donor (0.11 (6) electron). The distribution of density around the nickel atom is close to that predicted by ligand-field theory except for an anomalously low $3d_{xz}$ population and a large diffuse population, mainly in $4p_x$. This can be explained by invocation of configuration interaction, but the spectra of the system have not been sufficiently well examined to provide convincing evidence of this.

More detailed bonding models will be discussed in terms of this quantitative information and that arising from measurements of the spin density in the subsequent paper.

Acknowledgment. We are grateful to Associate Professor Allan White for his painstaking data collection and to Dr. E. N. Maslen for critical comments. This work was supported by funding from the Australian Research Grants Committee.

Registry No. $Ni(NH_3)_4(NO_2)_2$, 19362-26-6.

Supplementary Material Available: A list of observed and calculated structure factors (10 pages). Ordering information is given on any curent masthead page.

Covalent Bonding in *trans*-Tetraamminedinitronickel(II) Studied by Polarized Neutron Diffraction at 4.5 K

B. N. Figgis,*[1a] P. A. Reynolds,[1a] and R. Mason[1b]

Contribution from the School of Chemistry, University of Western Australia, Nedlands Australia 6009, and The School of Molecular Sciences, University of Sussex, Brighton, BN1 9QJ, England. *Received April 2, 1982*

Abstract: Magnetic structure factors (303) obtained from the polarized neutron diffraction experiment on $Ni(ND_3)_4(NO_2)_2$ are reported. They are analyzed by least-squares methods in terms of a model which employs the 3d and 4p orbitals of the nickel atom, sp hybrid orbitals on oxygen and nitrogen atoms, 1s orbitals on hydrogen atoms, and an "overlap" density in the Ni–N bonds. It is found that 27% of the spin of the molecule resides on the ligand groups, more on the nitro than the ammine. The nickel atom spin is, as expected, mainly in the e_g orbitals, but there is an appreciable spin in one of the 4p orbitals. There is strong evidence of σ-bonding interactions, including direct observation of the anticipated negative overlap populations. There is no evidence of π bonding. The results compare well with those obtained from the charge-density study. Together these two experiments allow a quite detailed account of the bonding in the complex, including that within the NO_2 groups, to be formulated. Comparison of the results with a simple MO/ligand-field theory is instructive, but it is obvious some features will only be reproduced by an extensive ab initio MO calculation. The spin distribution in the molecule is consistent with the weak magnetic exchange present in the compound, providing an exchange pathway including O···H–N hydrogen bonding is considered feasible.

In the preceding paper we presented an X-ray diffraction study of the electron density of *trans*-tetraamminedinitronickel(II). In this paper we present the spin density in this complex as determined by polarized neutron diffraction. We then discuss the implications of the results for the bonding in this first-row transition-metal complex with relatively covalent features.

Polarized neutron diffraction can be used to obtain magnetic structure factors $F_M(hkl)$ for paramagnetic crystals.[2] These are the Fourier components of the magnetization density, in the same way as X-ray diffraction structure factors are Fourier components of the electron density in the crystal. If the orbital contribution to the magnetization is small, which it is in this $^3A_{2g}$ ground-term complex, we can obtain from the F_M's a description of the spin density. The spin density is the *difference* between the charge densities of α and β spins. The electron density is, of course, the *sum* of these two quantities. Thus the techniques of X-ray diffraction and polarized neutron diffraction are entirely complementary.

For chemical interpretation, however, spin density has some advantage over electron density. Apart from spin-polarization effects, the only molecular orbitals to contribute to the spin density are the partially filled ones in the valence shell. The effect of the nonbonding core orbitals is small since they are very nearly spin paired. This is in contrast to charge density where a major contribution is from core orbitals which do not take part significantly in bonding. Bonding effects are, therefore, proportionately more obvious in the polarized-neutron than the X-ray diffraction experiment. This is often offset by the lesser precision and extent of the polarized neutron data.

The primary effect of chemical bonding in simple complexes is to transfer charge from ligand to metal via the doubly occupied bonding orbitals and from metal to ligand in the singly occupied antibonding orbitals. Overall there is a net *charge* transfer to the metal and a *spin* transfer from the metal ion onto the ligand. Since the spin transfer generally occurs within an antibonding molecular orbital, we expect to see three effects in the spin density in Ni-

(1) (a) University of Western Australia. (b) University of Sussex.
(2) (a) Brown, P. J.; Forsyth, J. B.; Mason, R. *Philos. Trans. R. Soc. London, Ser. B* **1980**, *290*, 481–495. (b) Figgis, B. N.; Reynolds, P. A.; Williams, G. A.; Mason, R.; Smith, A. R. P.; Varghese, J. N. *J. Chem. Soc., Dalton Trans.* **1980**, 2333–2338.

0002-7863/83/1505-0440$01.50/0